# NUMERICAL CONSIDERATION OF USING GEOTEXTILE IN DEFORMATION MECHANISM OF GROUND SURFACE DUE TO LIQUEFACTION OF SAND LENSES

**Babak Ebrahimian[1] & Yadolah Pashang Pisheh[2]**

*[1] School of Civil Engineering, University College of Engineering, University of Tehran, Tehran, Iran (e-mail: bebrahimian@ut.ac.ir)*
*[2] Department of Civil and Environmental Engineering, Amirkabir University of Technology, Tehran, Iran. (e-mail: pashang@aut.ac.ir)*

**Abstract:** Liquefaction of loose and saturated sand is one of the most important causes for damages during earthquake in areas near the sea. Even in many regions with proper soil characteristics, large deformation has been observed in the ground surface. In this paper, the behaviour of double sand lenses is investigated during earthquake and then the effects of using geotextile above these lenses for decreasing the deformation of ground surface due to liquefaction of sand lenses are studied by a series of two-dimensional finite difference analyses. The sand lenses, surrounding fine soil, and the geotextile were modelled in the seismic condition numerically. The liquefiable sand lenses and surrounding fine soil were simulated by employing the Finn-Byrne model and Mohr–Coulomb model respectively, while the geotextile reinforcements were modelled as cable elements. Verification analyses were conducted for validating the numerical model. In addition, some relatively comprehensive parametric studies were achieved on geotextile configuration.

**Keywords:** Geotextile, Seismic analysis, Numerical, Settlement, Sand, Reinforcement.

## INTRODUCTION

In many cases of heavy earthquakes, liquefaction has resulted in serious damages. The major reason of most damages and destructions related to San Francisco earthquake in 1906 was the liquefaction of loose saturated sand lenses that caused some landslides and ground failures inside and outside the city (Seed 1968). Similar damages happened due to liquefaction of sand lenses during Chile earthquake in 1960 (Fiegel and Kutter 1994), Alaska earthquake in 1964 (Fiegel and Kutter 1994), Washington earthquake in 1965 (Seed 1968) and also Guam earthquake in 1993. Loose sand lenses buried in fine soils is one of the cases which may result in these problems and is a weak point that can cause liquefaction during earthquakes. For soils, especially those consisting of loose saturated cohesionless material in seismically active areas, if drainage is unable to occur during the period of the loading sequence, then the tendency for volume reduction in each cycle of loading results in a corresponding progressive increase in pore water pressure. If the effective stress becomes zero and the sand loses its strength, the sand may be said to have liquefied, although this may be only a temporary state. Ground failure in the form of sand boils, lateral spreads and settlement are the common effects of liquefaction in soil deposits. However, in many regions with satisfactory soil classifications, large deformation has been observed in the ground surface. These areas that are situated near the seas contain some sedimentary layers of loose and comparatively uniform fine sand surrounded by clayey or silty soils. The deformation of these areas after earthquake is related to liquefaction of the sand layers, i.e. sand lenses. Vallejo (1988) and Holchin and Vallejo (1995) studied the mechanism of liquefaction of saturated sand lenses analytically and experimentally. Liu and Qiao (1984), considered the behaviour of layered sandy soils by cyclic loading using shaking table tests. Fiegel and Kutter (1994) investigated the liquefaction potential of sandy soils surrounded by silt layers due to earthquake loading by some centrifuge tests. Mir Mohammad Hosseinii and Nateghi (2001) studied the liquefaction mechanism of sand lenses numerically using the NISA program and considered the behaviour of lenses by a finite element model. They assumed the elasto-plastic behaviour for soils and used Drucher-Prager model. Pashang-Pisheh and Mir Mohammad Hosseinii (2005) considered the deformation mechanism of soils due to liquefaction of sand lenses during earthquake and assessed the critical depth in the liquefaction of sand lenses. They concluded that the critical depth is completely dependent on sand density and wave acceleration.

Soil improvement techniques are well-known methods to improve soft soils and to confront with soil weaknesses. The use of geotextile as an improvement method in many engineering applications has become more apparent and has proven to be an effective means of soil treatment to improve the performance of a reinforced fill layer placed on soft ground. The reinforcement that is strong in tension effectively combines with the soil that is strong in compression, forming a strong and semi-rigid composite material. Using soil reinforced with multiple layers of geotextile overlying a soft soil to increase the overall bearing and improved settlement performance is very common. There are many research works on the area of using geotextile to improve the bearing of soils and to reduce settelements with single layer of geotextile (Madhav and Poorooshasb 1988; Poorooshasb 1989, 1991; Ghosh and Madhav 1994; Shukla and Chandra 1994, 1995; Yin, 1997a, b, 2000; Maheshwari et al. 2004). Some studies on single layer reinforced system with finite element modelling to solve such problems are also reported in the literature (Love et al. 1987; Poran et al. 1989; Yin 1997a, 2000). Alawaji (2001) discussed the effects of reinforcing sand pad over collapsible soil and reported that successive reduction in collapse settlement up to 75% was obtained. British Rail Research (1998) has demonstrated that geotextile inserted in the ballast where tracks lie over soft ground can help extend maintenance intervals. The settlement mechanism of soils reinforced with geotextile above liquefied sand lenses during earthquake has not been investigated numerically yet. Many questions still remain as to the overall behaviour of the sand lenses

due to liquefaction and the mechanism of ground surface deformation caused by liquefying these lenses. Therefore, the object of this paper is to address the aspect of the liquefaction of sand lenses during earthquake, mechanism of ground surface deformation and settlement reduction through using optimum soil reinforcement with geotextile. The improving effects of geotextile for reinforcing the soil above such liquefiable sand lenses under seismic loading condition have been studied numerically by using FLAC commercial Package. The aim was to assess the seismic behaviour of sand lenses beneath the reinforced soil during earthquake with the variable parameter being the configuration of geotextile above the sand lenses.

## NUMERICAL MODELLING PROCEDURE

The two dimensional code, FLAC, was adopted for numerical analysis. FLAC program is capable of performing nonlinear analysis using a number of built-in constitutive models. Some of them are well-known models such as Mohr–Coulomb, Cam Clay and Ducker–Prager models. The program is widely used in geotechnical engineering applications and is attractive for seismic analysis of reinforced soil because it can model large distortions and near collapse conditions. A fully nonlinear analysis demands more user involvement and needs a comprehensive stress–strain model to reproduce some of the more various phenomena. FLAC is described as an explicit finite difference program that performs a Lagrangian analysis for solving the geomechanics problems. In this study 2-D plain strain analyses were performed. A fully coupled analysis was applied to model the behaviour of saturated soil under both static and dynamic loadings.

### Constitutive model for surrounding soils

Mohr-Coulomb constitutive model was used to model the behaviour of the soil. The failure envelope for this model corresponds to a Mohr-Coulomb criterion (shear yield function) with tension cutoff (tensile yield function). The stress-strain relationship is linear elastic-perfectly plastic. The linear behaviour is defined by elastic shear and drained bulk moduli. Also, the water bulk modulus is input along with these two elastic parameters. The shear modulus of soil is calculated with the formula given by (Seed and Idriss):

$$G_{max} = 1000 K_{2max} (\sigma')^{0.5} \quad (1)$$

Where $\sigma'$ is the mean effective confining stress in kPa and $G_{max}$ is maximum shear modulus in kPa. The Poisson's ratio is taken as 0.3. The non-associated plastic flow rule was assumed to have a more realistic prediction of the plastic volume change of the soil. The mechanical soil properties for surrounding clayey soils are summarized in Table 1.

**Table. 1.** Mechanical soil properties for surrounding clayey soils

| Soil type | $\gamma_{dry}$ $\left(kN/m^3\right)$ | $\gamma_{sat}$ $\left(kN/m^3\right)$ | $E$ $(MPa)$ | $C'$ $(kPa)$ | $\phi'$ $(^\circ)$ | $\nu$ | Porosity | $k$ $\left(cm/s\right)$ |
|---|---|---|---|---|---|---|---|---|
| **Clay** | 15 | 18 | 30 | 10 | 10 | 0.3 | 0.3 | $10^{-4}$ |

### Constitutive model for pore pressure generation in sand lenses

Under certain conditions, cyclic shear loading of sands may result in a tendency for volume reduction. For saturated sand the change of volume can occur only due to drainage. When drainage is not possible, the tendency for volume reduction will result in the development of excess pore pressure, which affects the behaviour of the sand by the change of effective stresses. The following empirical relation presented by Martin et al (1975) describes the incremental volumetric strain due to a cycle of simple shear loading on dry sand:

$$\Delta\varepsilon_{vd} = C_1 \left(\gamma - C_2 \varepsilon_{vd}\right) + \frac{C_3 \varepsilon_{vd}^2}{\gamma + C_4 \varepsilon_{vd}} \quad (2)$$

where $\Delta\varepsilon_v$ is the increment in volumetric strain that occurs over the current cycle, $\varepsilon_v$ is the accumulated volume strain for previous cycle, $\gamma$ is the shear strain amplitude for the current cycle, $C_1$ , $C_2$ , $C_3$ , $C_4$ are the constants dependent on the relative density of the sand. Equation (2) was modified by Byrne et al (1991) and the following simplified expression for the incremental volume strain was presented:

$$\Delta\varepsilon_{vd} = \gamma C_1 \exp\left(\frac{-C_2 \varepsilon_{vd}}{\gamma}\right) \quad (3)$$

Byrne proposed that the constant $C_1$ controls the amount of volume strain increment and $C_2$ controls the shape of the volumetric strain curve. It is logical to obtain these constants from volumetric strain data obtained from cyclic simple shear tests on the particular sand. Byrne demonstrated that when there is no such data attainable, the constants can be estimated using

$$C_1 = 7600 (Dr)^{-2.5} \quad (4)$$

$$C_2 = 0.4 / C_1 \quad (5)$$

Where Dr is the relative density of soil in present.

Byrne's formula is used to calculate irreversible volume changes during shaking, as this formulation is more general than the equation given by Martin. The FLAC program allows users to implement the new model cooperating with finite difference method. Therefore, due to the capability of implementation for the user-defined constitutive model, by applying the FISH function to the code FLAC, the massing rule was implemented into the Byrne' model to simulate the behaviour of liquefiable soil during seismic loading more accurately in the analysis. The procedure by which pore water pressures were calculated was such that: firstly the mechanical equilibrium equations were solved and plastic volumetric strain was estimated on the basis of occurred shear strain using a selected formulation, then the volume strain increments were applied as changes in normal strains to each saturated element. This method resulted in adjustment of effective stress and consequently, increases or decreases of pore water pressure. It is noticed that the normal strains in the horizontal and vertical directions were taken as one-third of the computed volume strain by formula. Also, considering that the equation proposed by Byrne for calculating irreversible volume change was developed according to results of cyclic simple shear tests, and as FLAC uses it for cases where both normal and shear strains take place, the corresponding maximum shear strain was used in formula in place of simple shear strain (Itasca 2001).

It was found by many numerical simulations with FLAC that using small values of relative density, such as 5% or 10% in formula given by Byrne, would lead to considerable computational difficulties and unacceptable results. So, in this research $C_1$ and $C_2$ were taken as 0.751 and 0.532, respectively. These constants which relate to *Dr= 40%* used in (4) and (5) found to yield more acceptable predictions. The dynamic properties of double sand lenses are presented in Table 2.

**Table. 2.** Dynamic properties of double sand lenses

| **Soil type** | $\gamma_{dry}\left(kN/m^3\right)$ | $\gamma_{sat}\left(kN/m^3\right)$ | $E\ (MPa)$ | $G_{\max}\ (MPa)$ | $B_{\max}\ (MPa)$ | $\phi'\ (^\circ)$ | $\nu$ | Dr% | $(N_1)_{60}$ |
|---|---|---|---|---|---|---|---|---|---|
| **Sand** | 14 | 20 | 15 | 58 | 125 | 28 | 0.3 | 40 | 7 |

**Cable element used as reinforcement**

The reinforcement was modelled using cable element as a linear, elastic–plastic element in FLAC program. Cable elements are one-dimensional axial elements with negligible compressive strength and an equivalent cross-sectional area of 0.0005 $m^2$. The equivalent linear elastic stiffness value for the reinforcement layers was taken as $E_s= 1\times 10^{10}$ . The yield strength of the reinforcement in all cases was kept constant at $T_y = 4\times 10^3$ kN/m; which is well above the magnitude of the maximum reinforcement load recorded in the simulations. Consequently, reinforcement rupture was not a possible failure mechanism in this study.

**Element size in dynamic analysis**

Numerical distortion of the propagating wave can occur in a dynamic analysis as a function of the modelling conditions. Both the frequency content of the input wave and the wave-speed characteristics of the system will affect the numerical accuracy of wave transmission. It was shown by Kuhlemeyer and Lysmer (1973) that for accurate representation of wave transmission through a model, the spatial element size, $\Delta L$ must be smaller than approximately one-tenth to one-eighth of the wavelength associated with the highest frequency component of the input wave, i.e.,

$$\frac{\lambda}{8} \le \Delta l \le \frac{\lambda}{10} \qquad (6)$$

Considering the above criterion, element size was defined small enough to allow seismic wave propagation throughout the analysis.

**Damping in dynamic analysis**

In analyses that use one of the plasticity constitutive models (e.g., Mohr-Coulomb), a considerable amount of energy dissipation can occur during plastic flow. Thus, for many dynamic analyses that involve large-strain, only a minimal percentage of damping may be required. Further dissipation will increase with amplitude for stress/strain cycles that involve plastic flow. The additional damping specified was 2 percent Rayleigh damping. It was applied at the natural frequency of the model (Itasca 2001).

**Numerical grid generation**

To generate the model, a grid was used with 100m length and 20m height as shown in Figure 1. Then, double sand lenses with 8m length and 4m free space were placed in the mentioned model. As shown in Figures 1 and 2, the ellipse geometry was chosen for sand lenses shape and the water table was specified at the ground surface elevation. So, sand lenses and surrounding fine soils were completely saturated. The dimensions and position of the double sand lenses are demonstrated in Figure 3.

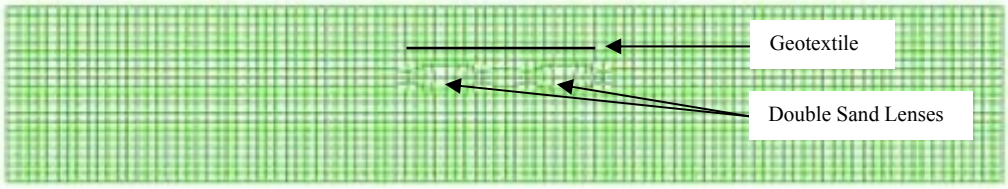


**Figure 1.** Numerical grid

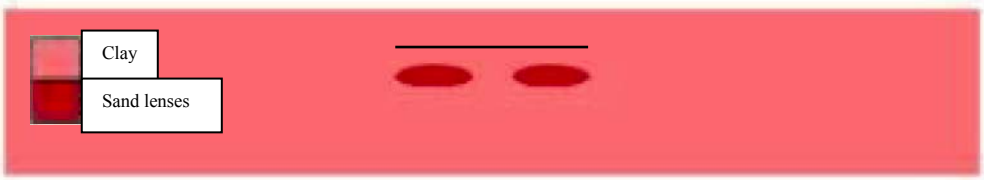


**Figure 2.** Locations of double sand lenses and surrounding clay soils

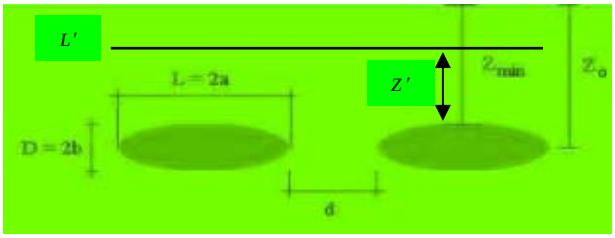


**Figure 3.** Dimensions of sand lenses (L=2a=8m; D=2b=2.66m; d=4m; $Z_o$=8m; $Z_{min}$=6.66m; $L'$=20m; $Z'$=1, 3, 6 and 7m)

**Seismic loading**

After static equilibrium was achieved (end of construction stage), the full width of the foundation was subjected to the variable-amplitude harmonic ground motion record. This seismic input motion was applied to the base of the numerical model (all nodes at the bottom) as a sine acceleration wave in x-direction corresponding to the xy-axes for the model. By adopting the amplitude of this wave, $a_{max}$ = 0.2g, the frequency, $f$ = 5 Hz, and duration, $t_d$ = 10 sec, the mechanism of sand lenses liquefaction and soil deformation due to this event was studied.

**NONLINEAR FULLY COUPLED STATIC AND DYNAMIC ANALYSIS AND DISCUSIONS**

Numerical methods relying on the discretization of a finite region of space require the appropriate conditions be enforced at the artificial numerical boundaries. In static analyses, fixed or elastic boundaries can be realistically placed at some distance from the region of interest. But in dynamic problems, however, such boundary conditions cause the reflection of upward propagating waves back into the model and do not allow the necessary energy radiation. So, by making use of FLAC program abilities, the boundary conditions were converted from simple to free-field boundaries. The boundary conditions at the sides of the model must account for the free-field motion which would exist in the absence of the structure. These conditions caused most of the energy in the wave reflected from side boundaries to be absorbed and the disorder of propagating waves to be prevented. In this way, plane waves propagating upward suffered no distortion at the boundary because the free-field grid provided conditions that were identical to those in an infinite model. The free-field model consisted of a one-dimensional "column" of unit width, simulating the behaviour of the extended medium. The height of the free field equalled the length of the lateral boundaries. It was discretized into ***n*** elements corresponding to the zones along the lateral boundaries of the FLAC zones.

**Verification**

A model including a liquefiable sand layer with surrounding clay soil that is completely saturated was analyzed to validate the numerical model and to verify the obtained results. Then, the behaviour of liquefied soil and the process of building up pore water pressure in the liquefied soil during the seismic loading were evaluated. So, a grid with a 100 m length and 20 m height was created with a 1 m element size as shown in Figure 4. The thickness of liquefiable layer as a loose sand was 2 m in the depth of 7 m of the model. The strength properties of clay and sand have been summarized in Table 1 and 2 respectively. At first, the static analysis of the model was conducted and the initial stress and pore water pressure in the model were computed. Therefore, the model subjected to its gravity forces was analyzed statically. The results obtained from this analysis are shown in Figures 5 to 7 as stress and pore pressure contours.


**Figure 4.** Clay and Sand layers in verification model

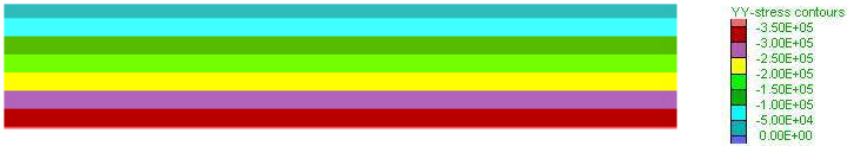


**Figure 5.** Initial vertical total stress distribution

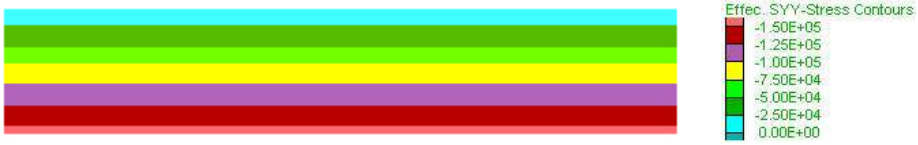


**Figure 6.** Initial vertical effective stress distribution

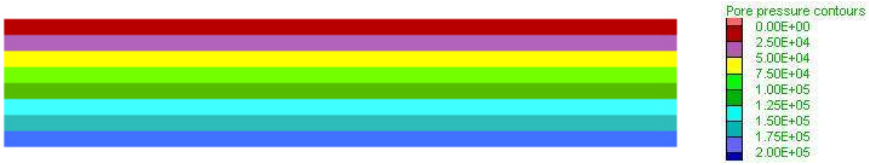


**Figure 7.** Initial pore pressure distribution

After the static analysis, the model came to equilibrium and gravity stresses became balance in the model. The unbalance forces resulting from gravity loading at grid points approached zero. At this stage, the model was prepared for dynamic analysis. The seismic excitation was applied to the base of the model with amplitude of $a_{max}$ = 0.3g, the frequency of $f$ = 5 Hz, and duration of $t_d$ = 10 sec till the sand layer became liquefied. The free field boundary was imposed to the lateral boundary of the model. The Byrne model defined the liquefiable sand layer. As it is shown in Figure 8, the effective stress in the sand layer tended to zero after 10 cycles of loading (t = 2 sec) and liquefaction occurred in sand soils. Also, the pore water pressure changes during cyclic loading are presented in Figure 9. It can be seen that the pore water pressure in sand layer increased during cyclic loading and after a maximum magnitude at t =2 sec of loading, reached a relatively constant level to the end of the loading.

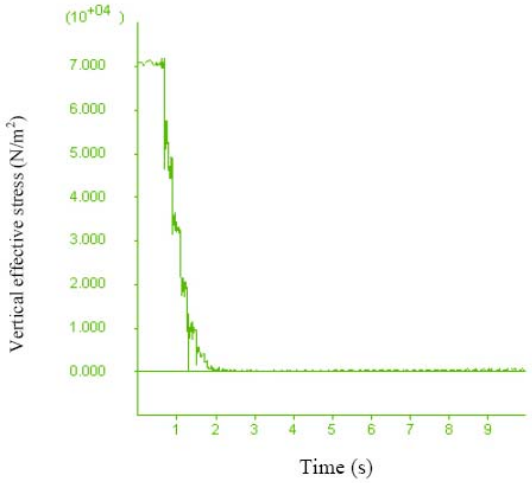


**Figure 8.** Vertical effective stress time history in sand layer

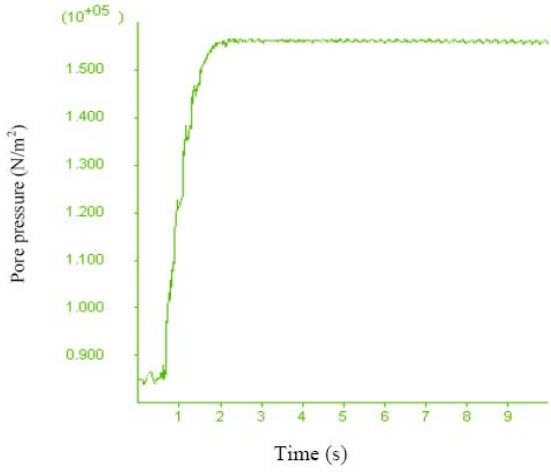


**Figure 9.** Pore pressure time history in sand layer

To represent the nonlinear stress-strain behaviour of soil more accurately by cyclic nonlinear models that followed the actual stress-strain path during cyclic loading, the massing behaviour was implemented into FLAC, which worked with Finn-Byrne model by a FISH subroutine. It included a backbone curve and a series of rules that governed unloading-reloading behaviour and stiffness degradation. A one-zone sample was analyzed with the modified Finn-Byrne model (with massing behaviour). The stress/strain loops for the one-zone sample for several cycles are shown in Figure 10 and hysteresis loops were modelled prior to the increase in shear strain in sand lenses as shown in Figure 10. It can be seen that shear modulus decreases with increasing shear strain. The hysteretic model seemed to handle multiple nested loops in a reasonable manner. There was clearly energy dissipation during seismic loading.

**Replacing reinforcements in numerical model**

Considering the plain strain conditions, a numerical simulation was conducted to investigate the behaviour of reinforced soil overlying on liquefied double sand lenses using FLAC program. The geotextile reinforcements were modelled as cable elements fully bonded with the surrounding soil, thus neglecting any slip. The effect of geotextile

on the vertical displacement above the sand lenses were obtained and discussed. Figures 11 and 12 represent vertical effective stress and pore water pressure contours respectively for the model that was not reinforced.

As it is shown in Figure 13, the effective stress in the sand lenses tended to zero after 2 sec from the beginning of cyclic loading and liquefaction occurred in the sand soils. Also, the pore water pressure changes prior to loading are presented in Figure 14. It can be seen that the pore water pressure in sand lenses increased during cyclic loading and after a maximum magnitude at t =2 sec of loading, obtained a relatively constant level to the end of loading.

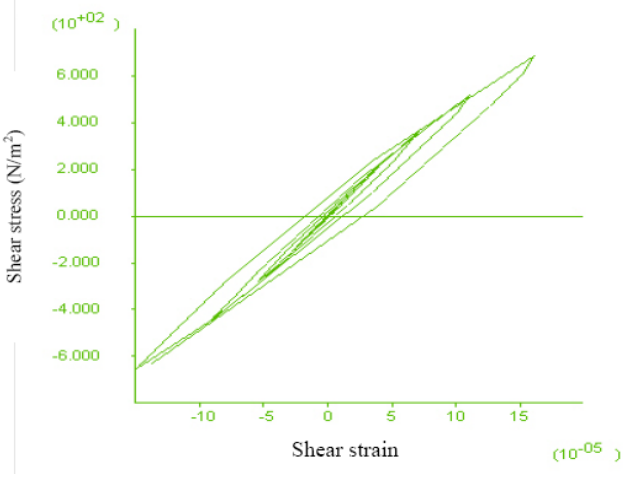


**Figure 10.** Hysteresis Loop obtained from One-zone sample exercised at several cyclic loading

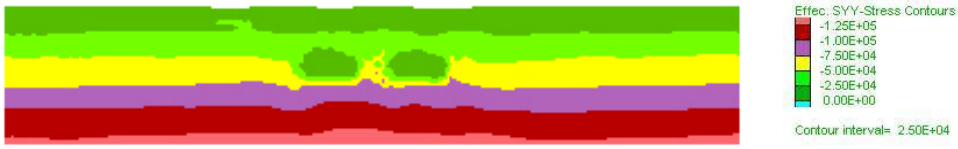


**Figure 11.** Vertical effective stress contours at the end of excitation

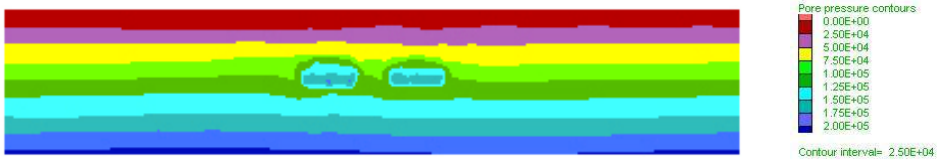


**Figure 12.** Pore water pressure contours at the end of excitation

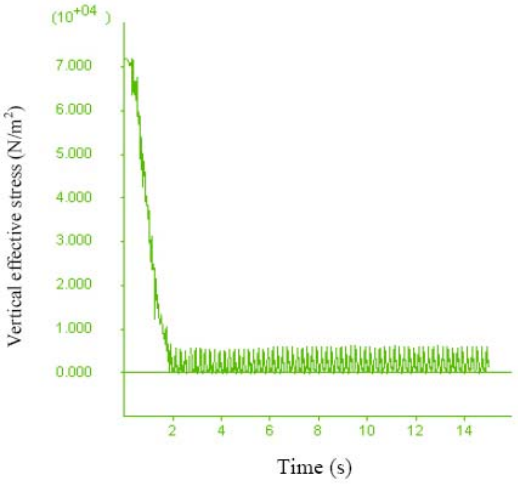


**Figure 13.** Vertical effective stress time history in sand lenses

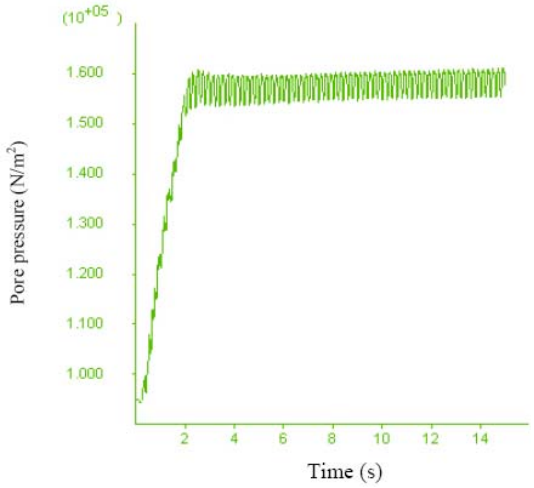


**Figure 14.** Pore pressure time history in sand lenses

The residual pore water pressure at the end of each cycle increased progressively with increasing number of cycles. The rate of pore water pressure development accelerated as liquefaction was approached; at which point strain amplitudes rapidly increased (Figure 15). The hysteresis loops were modelled prior to the increase in shear strain in sand lenses as shown in Fig. 16. It can be seen that shear modulus decreased with increasing shear strain and at the end of loading.

A number of parametric study were carried out in order to assess the effect of using geotextile reinforcement on the deformation of soils above double liquefied sand lenses due to liquefaction of these lenses. In these series, the depth of replaced geotextile with length of 20m (from the beginning of first sand lens to the end of second sand lens) was varied. Four variations were considered for the position of geotextile from the top level of sand lenses (1m, 3m, 6m and 7m above the sand lenses level). Typical variations of vertical displacement with depth above the sand lenses level in company with reinforced soil upon these sand lenses are shown in Figures 17 and 18. The vertical displacement at the centreline of the double sand lenses from top level of these lenses is presented in Figure 17, while the vertical displacement at the centreline of one of the sand lenses from the top level of this lens is shown in Figure 18.

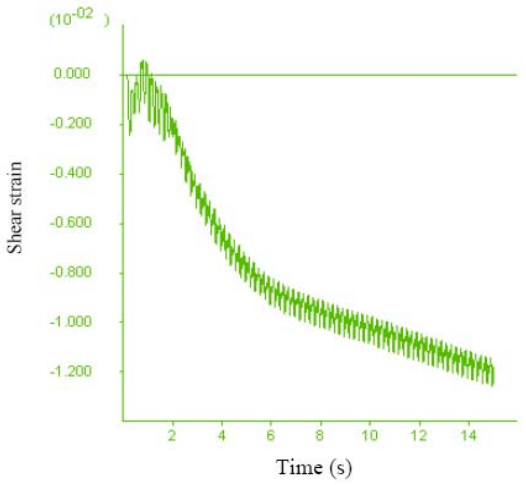


**Figure 15.** Shear strain time history in sand lenses during cyclic loading

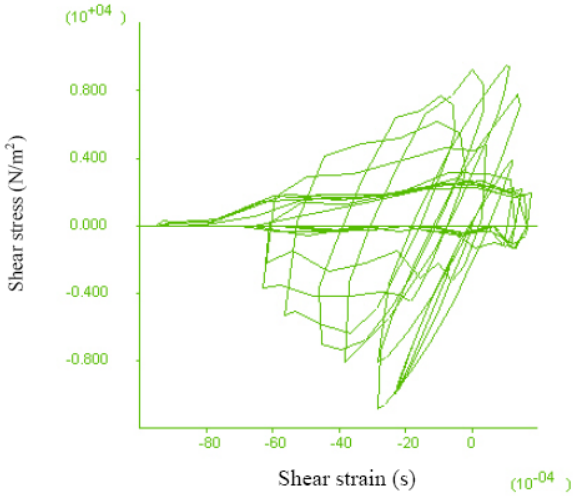


**Figure 16.** Shear strain time history in sand lenses during cyclic loading

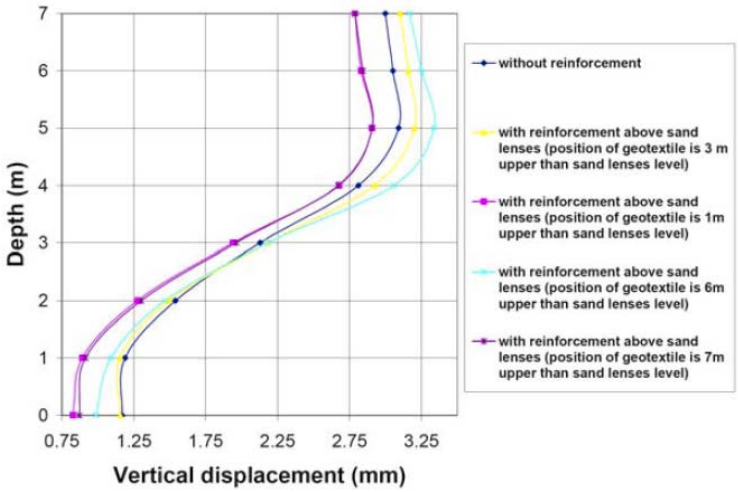


**Figure 17.** Vertical displacement at centreline between sand lenses at the end of cyclic loading

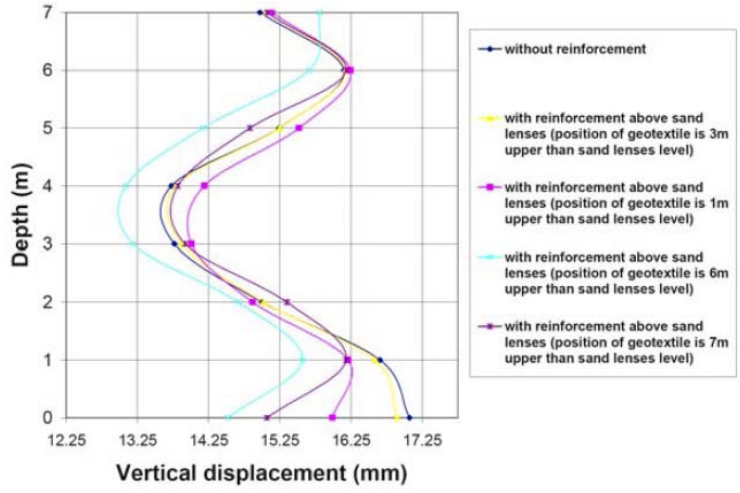


**Figure 18.** Vertical displacement at centreline of one of sand lenses at the end of cyclic loading

Figure 17 shows that vertical displacement at the centreline of sand lenses (above the liquefied lenses level) decreased by using geotextile as a reinforcement and the geotextile layer has an optimum depth. Figure 17 demonstrates that when the geotextile layer was 6m above the sand lens; the vertical displacement was more than other conditions. It is noted that in the latter case, if the geotextile was placed at the ground surface or 1m above the top level of sand lenses, the most deduction was observed. To highlight the beneficial effect of using reinforcement layer on the settlement reduction, the quantities of vertical displacement are summarized in Tables 3 and 4 for all cases.

**Table. 3.** Comparison between the obtained results in between the two sand lenses

| | **1m above the sand lenses** | **3m above the sand lenses** | **6m above the sand lenses** | **7m above the sand lenses** | **Without reinforcement** |
|---|---|---|---|---|---|
| **Vertical displacement at ground surface** | 2.789mm | 3.104mm | 3.167mm | 2.789mm | 3mm |
| **Vertical displacement at top of the sand lens** | 0.827mm | 1.156mm | 0.988mm | 0.871mm | 1.169mm |

**Table. 4.** Comparison between the obtained results for the centreline of one of the sand lenses

| | **1m above the sand lenses** | **3m above the sand lenses** | **6m above the sand lenses** | **7m above the sand lenses** | **Without reinforcement** |
|---|---|---|---|---|---|
| **Vertical displacement at ground surface** | 15.14mm | 15.07mm | 15.81mm | 15.07mm | 14.97mm |
| **Vertical displacement at top of the sand lenses** | 15.99m | 16.9mm | 14.52mm | 15.07mm | 17.07mm |

To define the optimum depth for placing the geotextile above the sand lenses, a set of analyses were conducted and from the obtained results, the vertical displacements for the above two positions were computed and plotted against the position of geotextile layer from the top level of sand lenses in Figures 19 and 20. Figure 19 shows that the optimum depth of geotextile in the centreline of the two sand lenses is 1m or 7m (ground surface level) from the top level of sand lenses and Figure 20 shows that the optimum depth of geotextile in the centreline of one of the sand lenses is about 4.5m from the top level of sand lens.

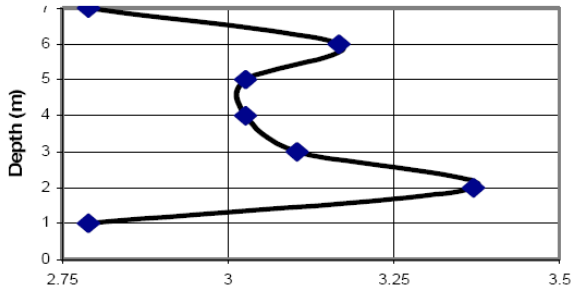


**Figure 19.** Vertical displacement at ground surface at centreline of two sand lenses

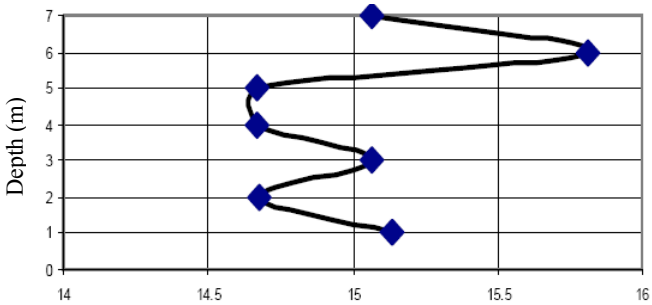


**Figure 20.** Vertical displacement at ground surface at centreline of one of sand lenses

## CONCLUSIONS

In this paper, mechanism of deformation of reinforced soil using geotextile overlaying liquefied double sand lenses was studied. Based on the results obtained from this investigation, the following conclusions can be drawn:

1. The present study demonstrates a successful application of FLAC in analyzing the response of reinforced soil placed over the liquefied double sand lenses.
2. After liquefaction in sand lenses occurred, a bowled settled media in the middle of double sand lenses is established.
3. The maximum magnitude of soil settlement occurs near the liquefied lenses.

4. Soil improvement of soft clay above the liquefied double sand lenses significantly decreases the vertical displacement of clay soil.
5. The analyses of the observed results show that for the soil column between two sand lenses, the optimum depth for geotextile (in the centreline of two sand lens) was 1m or 7m (ground surface level) and in the centreline of one of sand lenses was about 4.5m from the top level of sand lens.

**Corresponding author:** Mr Babak Ebrahimian, School of Civil Engineering, University College of Engineering, University of Tehran, 11365 - 4563, Enghelab St., Tehran, Iran. Tel: 0098-61112181. Email: bebrahimian@ut.ac.ir.

**REFERENCES**

Alawaji, H. 2001. Settlement and bearing capacity of geogrid-reinforced sand over collapsible soil. Geotextiles and Geomembranes, Vol. 19, PP. 75–88.

British Rail Research, 1998. Supporting roll—geogrids provide a solution to railway track ballast problems on soft and variable subgrades. Ground Engineering, Vol. 31, No. 3, PP. 24–27.

Byrne, P. 1991. A cyclic shear-volume coupling and pore-pressure model for sand. Proceedings of Second International Conference on Recent Advances in Geotechnical Earthquake Engineering and Soil Dynamics, St. Louis, Missouri, March, Paper No. 1.24, PP. 47-55.

Fiegel, G.L. and Kutter, B.L. 1994. Liquefaction mechanism for layered soils. Journal of Geotechnical Engineering Div., ASCE, Vol. 120, No. 4, PP. 737-755.

Ghosh, C. and Madhav, M.R. 1994. Settlement response of a reinforced shallow earth bed. Geotextile and Geomembranes, Vol. 13, No. 9, PP.643–656.

Holchin, J.D. and Vallejo, L. 1995. The liquefaction of sand lenses due to cyclic loading. Proceeding of 3rd International Conference on Recent Advances in Geotechnical Earthquake Engineering and Soil Dynamics, Vol. I, Missouri, PP. 253-259.

Kuhlemeyer, R. L. and Lysmer, J. 1973. Finite element method accuracy for wave propagation problems. Journal of Soil Mechanics and Foundations Div., ASCE, Vol. 99(SM5), PP. 421-427.

Liu, H. and Qiao, T. 1984. Liquefaction potential of saturated sand deposits underlying foundation of structures. Proceeding of Eight World Conference of Earthquake Engineering III, San Francisco, California, PP. 199-206.

Love, J.P., Burd, H.J., Milligan, G.W.E. and Houlsby, G.T. 1987. Analytical and model studies of reinforcement of a layer of granular fill on soft clay subgrade. Canadian Geotechnical Journal, Vol. 24, PP. 611– 622.

Madhav, M.R. and Poorooshasb, H.B. 1988. A new model for geosynthetic- reinforced soil. Computers and Geotechnics, Vol. 6, No. 4, PP.277–290.

Maheshwari, P., Basudhar, P.K. and Chandra, S. 2004. Analysis of beams on reinforced granular beds. Geosynthetic International, Vol. 11, No. 6, PP. 470–480.

Martin, G. R., Finn, W. D. L. and Seed, H. B. 1975. Fundamentals of liquefaction under cyclic loading. Journal of Geotechnical Engineering Div., ASCE, Vol. 101(GT5), PP. 423-438.

Mir Mohammad Hosseinii, S.M. and Nateghi, F. 2001. The crack development due to liquefaction of sand lenses during earthquake loading. Proceeding Fourth International Conference on Recent Advances in Geotechnical Earthquake Engineering and Soil Dynamics, San Diego, California, PP. 407-413.

Pashang Pisheh, Y. and Mir Mohammad Hosseinii, S.M. 2005, Investigation of Liquefaction Mechanism in Double Sand Lenses. Electronic Journal of Geotechnical Engineering, No. 0552.

Poorooshasb, H.B. 1989. Analysis of geosynthetic reinforced soil using a simple transform function. Computers and Geotechnics, Vol. 8, No. 4, PP.289–309.

Poorooshasb. H.B. 1991. On mechanics of heavy reinforced granular mats. Soils and Foundations, Vol. 31, No.2 , PP.134–152.

Poran, C.J., Herrmann, L.R. and Romstad, K.M. 1989. Finite element analysis of footing on geogrid-reinforced soil. Proceeding of geosynthetics, San Diego, USA, PP. 231–242.

Seed, H.B. 1968. Landslides during earthquake due to soil liquefaction. Journal of the Soil Mechanics and Foundation Div., ASCE, Vol. 94, SM5, PP. 1053-1112.

Shukla, S.K. and Chandra, S. 1994. A study of settlement response of a geosynthetic-reinforced compressible granular fillsoft soil system. Geotextile and Geomembranes, Vol. 13, No. 9, PP.627–639.

Shukla, S.K. and Chandra, S. 1995. Modeling of geosynthetic-reinforced engineered granular fill on soft soil. Geosynthetic International, Vol. 2, No. 3, PP. 603–617.

Itasca, FLAC "Fast Lagrangian Analysis of Continua", Theory Manual, 2001.

Vallejo, L. 1988. The liquefaction of sand lenses during an earthquake. Proceeding of Earthquake Engineering and Soil Dynamics II- Recent Advances in Ground Motion Evaluation, ASCE New York, PP. 493-507.

Yin, J.H. 1997a. Modeling geosynthetic-reinforced granular fills over soft soil. Geosynthetic International, Vol. 4, No. 2, PP. 165–185.

Yin, J.H. 1997b. A non-linear model for geosynthetic-reinforced granular fill over soft soil. Geosynthetic International, Vol. 4, No. 5, PP.523– 537.

Yin, J.H. 2000. Comparative modeling study on reinforced beam on elastic foundation. Journal of Geotechnical and Environmental Engineering, ASCE, Vol. 126, No. 3, PP. 265–271.